Fault Localization and Functional Testing of ICs by Lock-in Thermography

O. Breitenstein, J.P. Rakotoniaina, F. Altmann*, J. Schulz, G. Linse****
Max Planck Institute of Microstructure Physics, Weinberg 2, D-06120 Halle, Germany
E-Mail: breiten@mpi-halle.de
*Fraunhofer Institute for Mechanics of Materials, Heideallee 19, D-06120 Halle, Germany
**Melexis GmbH, Haarbergstraße 67, D-99097 Erfurt, Germany

Abstract

In this paper new thermographic techniques with significant improved temperature and/or spatial resolution are presented and compared with existing techniques. In infrared (IR) lock-in thermography heat sources in an electronic device are periodically activated electrically, and the surface is imaged by a free-running IR camera. By computer processing and averaging the images over a certain acquisition time, a surface temperature modulation below 100 µK can be resolved. Moreover, the effective spatial resolution is considerably improved compared to stead-state thermal imaging techniques, since the lateral heat diffusion is suppressed in this a.c. technique. However, a serious limitation is that the spatial resolution is limited to about 5 microns due to the IR wavelength range of 3 -5 µm used by the IR camera. Nevertheless, we demonstrate that lock-in thermography reliably allows the detection of defects in ICs if their power exceeds some 10 µW. The imaging can be performed also through the silicon substrate from the backside of the chip. Also the well-known fluorescent microthermal imaging (FMI) technique can be be used in lock-in mode, leading to a temperature resolution in the mK range, but a spatial resolution below 1 micron.

Introduction

Fault localisation in integrated circuits is the essential starting point for an aimed structural and morphological failure analysis with FIB-, SEM or TEM. Liquid crystal investigations (LC, [1]) and fluorescent microthermal imaging (FMI, [2]) are standard thermal fault localization techniques, which can be used to detect defects connected with local heat generation in ICs such as oxide breakdown, latch-up, or metallization shorting. Steady-state infrared (IR) thermography is also sometimes used for this purpose, but it has two main disadvantages: Its spatial resolution is limited to about 5 µm owing to the wavelength range used by the technique, and it shows a strong IR-emissivity contrast (ε-contrast), which makes metallized areas appear dark and obscures the thermal contrast. In principle the ε-contrast may be compensated by capturing and processing additional images at elevated temperatures [3], but this is a time-consuming and complicated procedure and often meets with limited success. On the other hand, contrary to LC and FMI imaging, IR investigations can be easily performed from the backside of the chip, which is the only way to investigate ICs in flip-chip mounting. It shares this advantage with light emission microscopy (LEM, [3]), which, however, does not image resistive heat sources like metallization shorts. The detection limit of all previously discussed thermal methods is limited to 20 - 100 mK. Hence, they only allow to image the mentioned pronounced heat sources, but as a rule not regions of the normal operation of an IC. Decreasing operation voltages, multiple metallization layers, and new package technologies complicate the use of standard fault localisatation techniques, like light emission microscopy and liquid crystal thermography.

It will be shown that the IR lock-in thermography technique considerably lowers the thermal detection limit to below 0.1 mK [4] and eliminates the ε-contrast with a single measurement by displaying the phase image. The thermal diffusion length depends on the lock-in frequency and is between 3 and 1 mm for the lock-in frequencies of 3 - 30 Hz used here. However, this is no limit for the effective spatial resolution, which also depends on the geometry and the location of the heat sources. Point-like heat sources at the surface can be located to an accuracy of one pixel, and also the extension of the halo, which exists esp. around extended heat sources, is usually smaller than the thermal diffusion length, but considerably depends on the lock-in frequency, as Fig. 3 will show. IR lock-in thermography is very easy to apply and is also commercially available now [5]. In addition, sub-micron spatial resolution can be obtained by performing FMI in lock-in (a.c.) mode, which is currently under development. We are introducing here first results of Lock-in FMI with 0.5 µm spatial resolution.

Experimental

The technique of IR lock-in thermography has been used mostly for non-destructive testing and thermo-elastic investigations [6], as well as for the investigation of shunts in solar cells [7]. Periodic heat pulses are generated in the sample by pulsing the power supply to the IC. The surface is imaged by a free-running thermocamera, and all pixel information is digitally processed on-line to perform a two-phase lock-in correlation, phase-referred to the periodic heating. Hence, the primary results of lock-in thermography are the in-phase (0°-) image and the quadrature (90°-) image. They may be converted into the amplitude image, displaying the local temperature modulation amplitude, and the phase image, which essentially describes the time delay of the local temperature modulation referred to the periodic power supply pulse. While the amplitude signal still contains the ε-contrast, the phase image is principally independent on the local value of the emissivity. By averaging over many lock-in periods the signal-to-noise ratio (SNR) of a lock-in measurement drops significantly below the SNR of the primary signal.

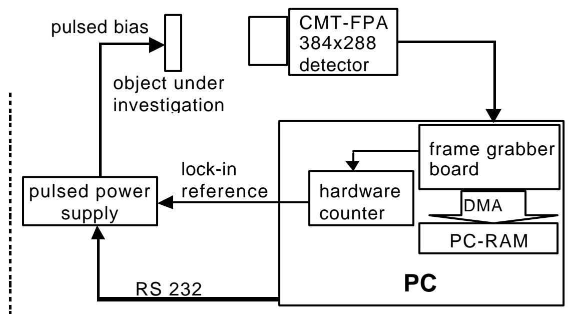

Fig. 1: Scheme of the TDL 384 M 'Lock-in' thermography system

The lock-in thermography system used to take the data included in this paper was the TDL 384 M Lock-in from Thermosensorik GmbH, Erlangen Germany [5] shown in Figure 1. It is based on a highly sensitive 384x288 pixel sized Stirling-cooled HgCdTe (MCT) focal plane array (FPA) IR detector head made by AIM, Heilbronn (Germany) [8], which detects at 3 -5 µm wavelength at a full frame rate of up to 140 Hz. The digital image information (14 Bit) is captured by a frame grabber board and transmitted on-line by DMA to the RAM of a 2x800 MHz Dual Pentium III PC. The PC performs the lock-in correlation and controls the hardware for generating the lock-in reference signal, which triggers the pulsed power supply. The detector head may be equipped with a 28 mm standard IR objective, providing a pixel resolution down to 30 µm, or by different special microscope objectives, providing a pixel resolution down to 5 µm. The temperature noise level of this system decreases with the square root of the acquisition time and reaches a level of about 70 µK after 1000 s (17 min). The digital lock-in correlation procedure used in this system is explained in Fig. 2 [4].

Additionally, we have modified a digital fluorescent microthermal imaging (FMI) system to work in lock-in mode. Here we exploit the natural 100 Hz flickering of the UV lamp of the FMI optical microscope. The supply voltage of the sample is pulsed at 100 Hz, phase-synchronously to the mains frequency, and the fluorescence signal is averaged over many lock-in periods by a cooled slow-scan CCD camera. Using special hardware, the phase between the UV light pulses and the supply voltage pulses is changed by 90° for successively captured images, so that 4 subsequent fluorescence images correspond to a phase difference between light- and bias pulses of 0°,

Fig. 2: Principle of the lock-in correlation procedure [4]: The pixel information of each incoming frame is multiplied in two channels by different sets of weighting factors, approximating in channel 1 a sin and in channel 2 a -cos function. After summing up the results in two frame storages over many periods, storage 1 contains the in-phase (0°) image and storage 2 the quadrature (-90°) image, which may be converted into the amplitude- and the phase image.

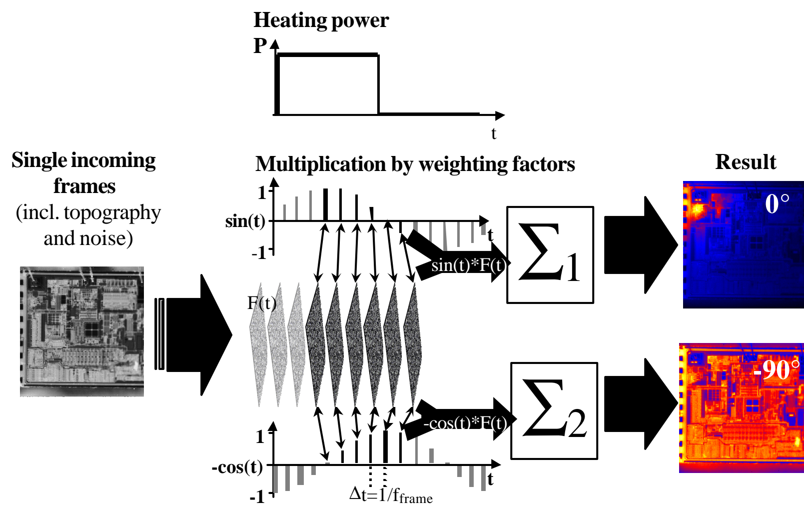

90°, 180°, and 270°. From these four images the temperature modulation amplitude signal A and the phase signal Φ are calculated for every pixel position by:

$$A = \sqrt{\left(I^{0°} - I^{180°}\right)^2 + \left(I^{90°} - I^{270°}\right)^2} \quad (1)$$

$$\Phi = \arctan\left(\frac{\left(I^{90°} - I^{270°}\right)}{\left(I^{0°} - I^{180°}\right)}\right) \quad (2)$$

In principle this is a heterodyne technique, since the fluorescence signal is the product of the UV intensity and the (temperature dependent) quantum efficiency of the dye. Therefore the total amount of light, averaged over many periods, contains some amplitude and phase information about the periodic temperature modulation at 100 Hz. By performing the pairwise differences in the brackets of (1) and (2), the part of the fluorescence signal, which is not affected by temperature modulation, completely cancels out. Also here, by averaging over many images the noise level may be considerably reduced.

For the comparison with other techniques Light Emission Microscopy (LEM) has been performed using an astronomical Peltier-cooled CCD-camera AlphaMaxi from OES GmbH Egloffstein (Germany) with Kodak-chip KAF1600 in combination with a Mitutoyo FS-70 microscope. The photo integration times are indicated in the images. Liquid crystal investigations have been performed using nematic liquid crystals with a clearing point of 29°C under the Mitutoyo FS-70 in cross-polarization modus. The sample temperature was regulated manually by a hairdryer.

Results
IR Lock-in thermography

For lock-in thermography on ICs until now only amplitude images have been published [4]. Fig. 3 shows an IR topography image (which is a single IR image, always measured before a lock-in measurement), and amplitude- and phase images of an intact integrated circuit in static operation with the supply voltage of 16 V / 2.4 mA pulsed at 3 and 20 Hz. Though also the topography image was measured with supply voltage applied, the emissivity contrast dominates this image and does obscure the weak heat sources. In the amplitude images the stationary topography contrast is compensated and the dominant heat sources can be located. However, this image is still modulated by the ε-contrast, and it is hard to decide whether some bright features are weak local heat sources or regions of high IR emissivity. The phase image, on the other hand, is totally free of emissivity contrast and clearly shows single heat sources. The influence of the lock-in frequency on the extension of the inevitable halos around heat sources is clearly visible both in the amplitude and in the phase images. Moreover, it is visible that in the phase image heat sources of different power appear with a similar brightness.

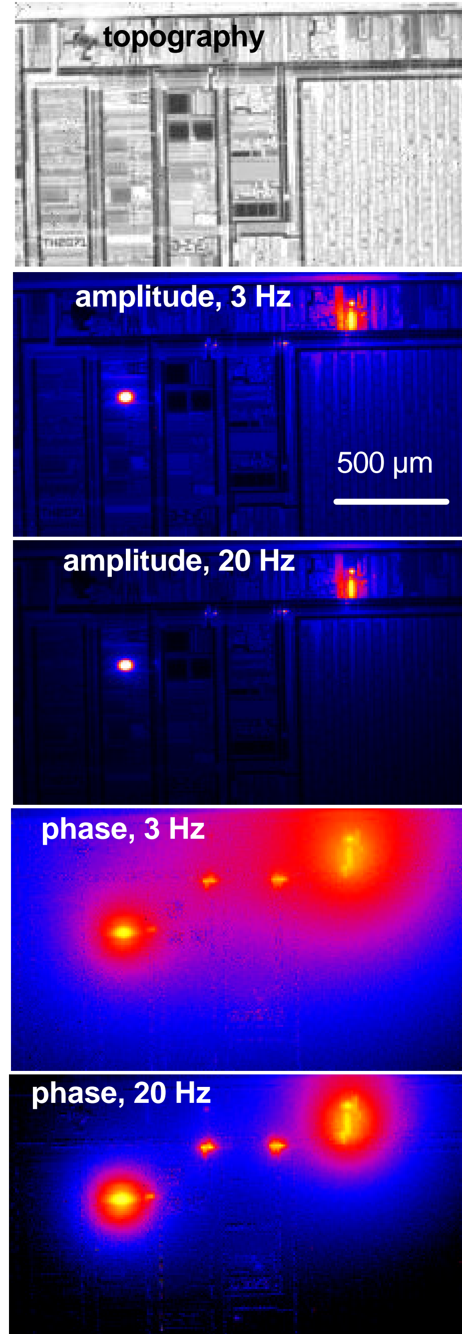

Fig. 3: Topography, amplitude-, and phase images of an IC in pulsed static operation for two lock-in frequencies

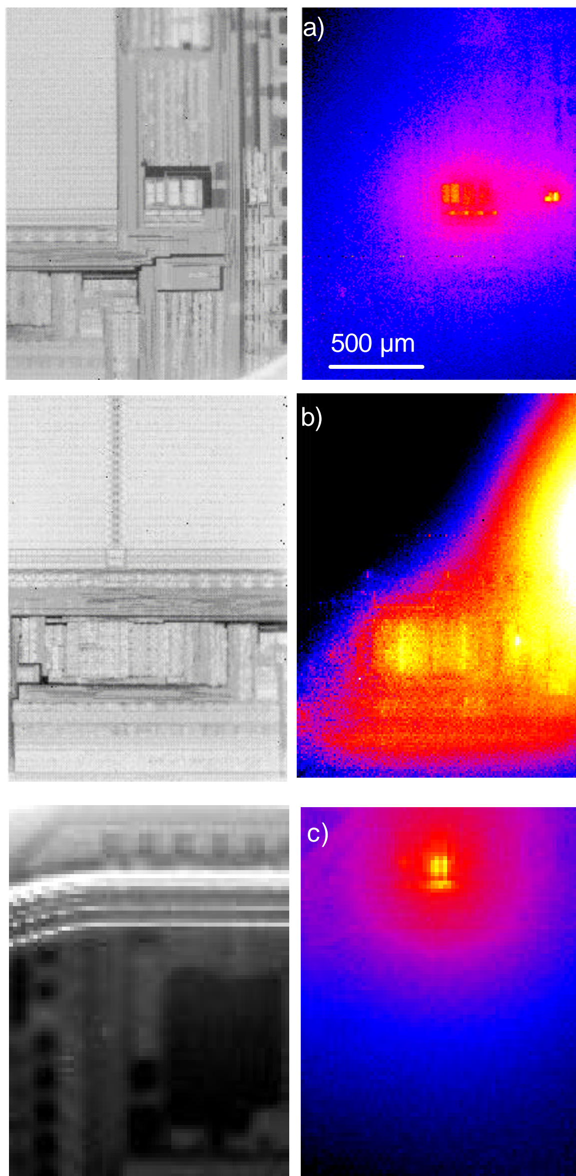

Fig. 4: Topography and phase images of 3 positions in an 8 bit microprocessor clocked at 12 MHz, supply voltage pulsed at 20 Hz, imaged "through the chip" from the opened backside. The defect in position c) is responsible for the increased supply current.

Topography and phase images from the investigation of 3 positions in an 8 Bit microprocessor IC are shown in Fig 4. This IC was working in dynamic operation with the internal clock generator of 12 MHz running, but no ROM was connected. The supply voltage of 5 V was pulsed at 20 Hz. We have investigated an intact IC consuming a current of about 8 mA, and a defective one taking about 50 mA at 5 V. The investigations have been performed from the opened backside of the chip, as it has to be done if chips are mounted in "flip chip" configuration. The heat sources in the upper images a) and b) of Fig. 4 with a maximum amplitude of about 10 and <1 mK, respectively, belong to the normal operation of this IC. They are found both in an intact IC consuming 8 mA supply current and in the defective one. The dominant heat source in Fig. 4 c), however, showing an amplitude of about 1 K, is the fault location. In an intact sample no measurable heat is produced in this position. While the acquisition times for Fig. 4 a) and b) were 2 and 20 min, respectively, Fig. 4 c) has been recorded within some seconds

The final example shown in Fig. 5 demonstrates the high sensitivity of the lock-in thermography technique. This was a CMOS device damaged by ESD pulses, which showed a leakage current of about 24 µA at an applied bias of 5.5 V, leading to a dissipated power of 132 µW. The device was measured under these conditions with a lock-in frequency of 3 Hz for an acquisition time of t_{ac} = 7 min. The maximum measured T-modulation signal amplitude in defect position was about 500 µK, and the signal-to-noise ratio (SNR) was about 4, hence the noise level of this measurement was in the order of 125 µK. Since the noise level decreases with $1/\sqrt{t_{ac}}$ [4], after 1 hr acquisition time a heat source of the same geometry with a power of 45 µW could be detected with the same SNR. Note that this heat source seems to have a certain spatial extension. For a real point source at the surface the detection limit would be even lower.

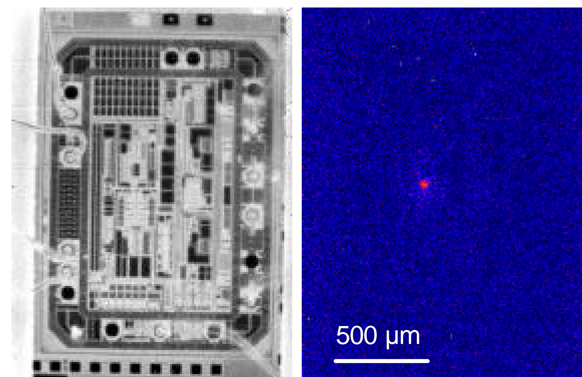

Fig. 5: Topography and amplitude image of a defect in an IC dissipating 132 µW, measured at 3 Hz with an acquisition time of 7 minutes

Meanwhile we have performed about 40 fault localizations in different IC types by IR lock-in thermography, hitherto all of them being successful. In some cases the fault origin was verified using FIB cross section preparation of the fault region followed by TEM failure analysis. Whenever a fault results in a current increase of at least some ten microamps, it usually can be localized by this technique to a spatial accuracy of 5 ... 10 µm.

Lock-in FMI

Fig. 6 shows one of our first results of Lock-in FMI. Here an NMOS test structure with an oxide breakdown was investigated, leading to a leakage current of 6.5 mA at 5 V. Also here the "topography image" (a single fluorescence image) was captured with a bias applied to the structure, showing a weak quenching of the fluorescence in fault position. After <10 minutes acquisition time of Lock-in FMI, the amplitude image clearly shows the point-like fault position as well as a resistively heated line. The pixel resolution in these images is 0.5 µm. Indeed, the bright local signal maximum in fault position is significant and defined by this spatial resolution.

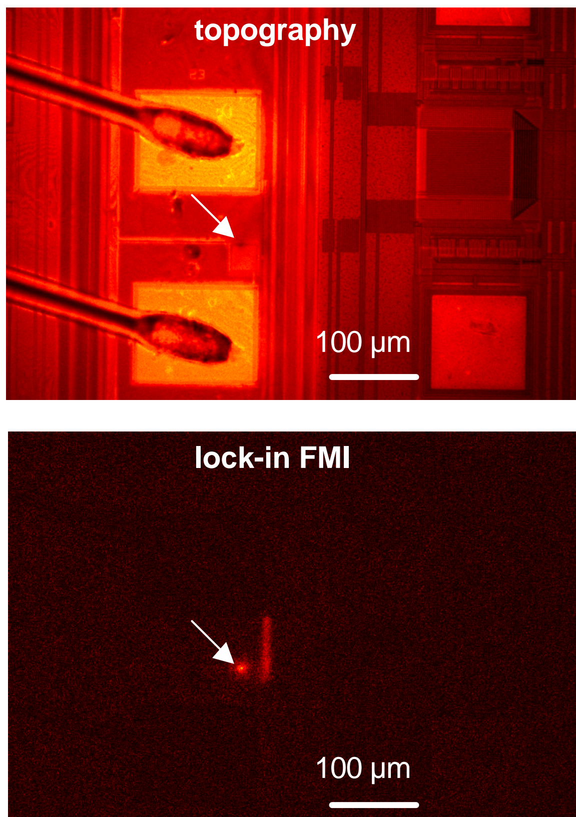

Fig. 6: Fluorescence image (topography, top) and lock-in FMI amplitude image (bottom) of a MOS test structure containing an oxide breakdown (arrows) and a resistively heated line.

Comparison with other techniques

The IC investigated in this section (in some images called device #3) was the same IC which was also used for Fig. 3. It was a High-Voltage-CMOS motor controller, which was damaged by ESD pulses. The undamaged IC shows a quiescent current of about 40 µA and no light emission. Due to the damage the quiescent current has increased to about 1 mA at Vcc = 10V and about 2.8 mA at Vcc = 16 V.

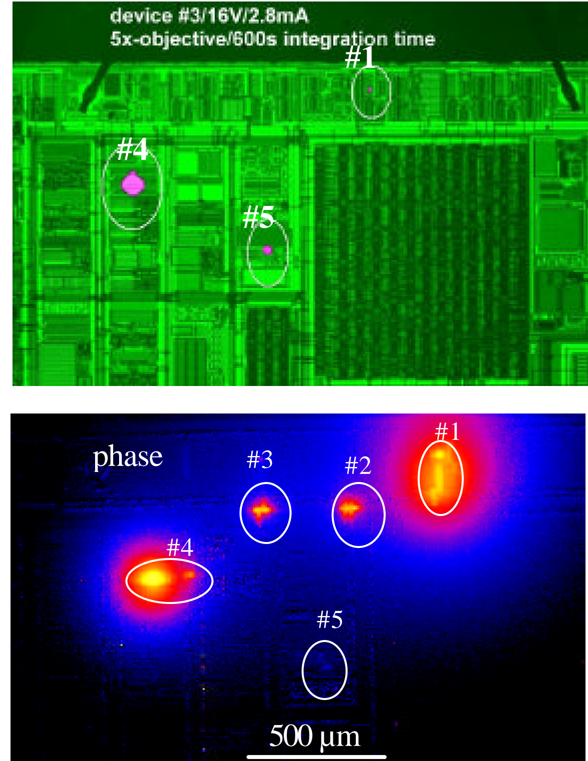

Fig. 7: Comparison between light emission image (top: green = topography, red = light emission) and lock-in thermography (phase image, bottom, see Fig. 3) of an ESD pulse damaged High-Voltage-CMOS motor controller

Fig. 7 shows a survey light emission image of the defective sample at Vcc = 16 V and the amplitude image and the phase image of the IR lock-in thermography investigation of the same circuit under the same conditions. The LEM results are displayed as a superposition of the topography image (in green color) and the light emission image in red color. Different positions are indicated as #1 through #5. Note that in the amplitude image (see Fig. 3) the signal amplitude is proportional to the dissipated power, and metallized regions appear darker due to their low IR emissivity (emissivity contrast). The phase image, on the other hand, is a measure of the time delay of the local T-modulation with respect to the modulated applied bias. So this image does not contain the emissivity contrast, and heat sources of different power may appear with a comparable brightness. Note that the defect in position #4 shows a T-modulation amplitude above the brightness scaling limit, therefore this defect appears artificially blurred in the amplitude

image. The comparison shows that some local heat sources detected by IR lock-in thermography in positions #2 and #3 and also the lower part in position #1 are not visible in light emission. On the other hand, one light emission site (position #5) is only weakly visible in thermography (only in the phase image). Obviously the sites visible only in thermography are purely resistive heat sources, whereas the light source in position #5 seems to be connected with a very weak heat dissipation. Generally, the spatial resolution of light microscopy is clearly superior to that of IR lock-in thermography.

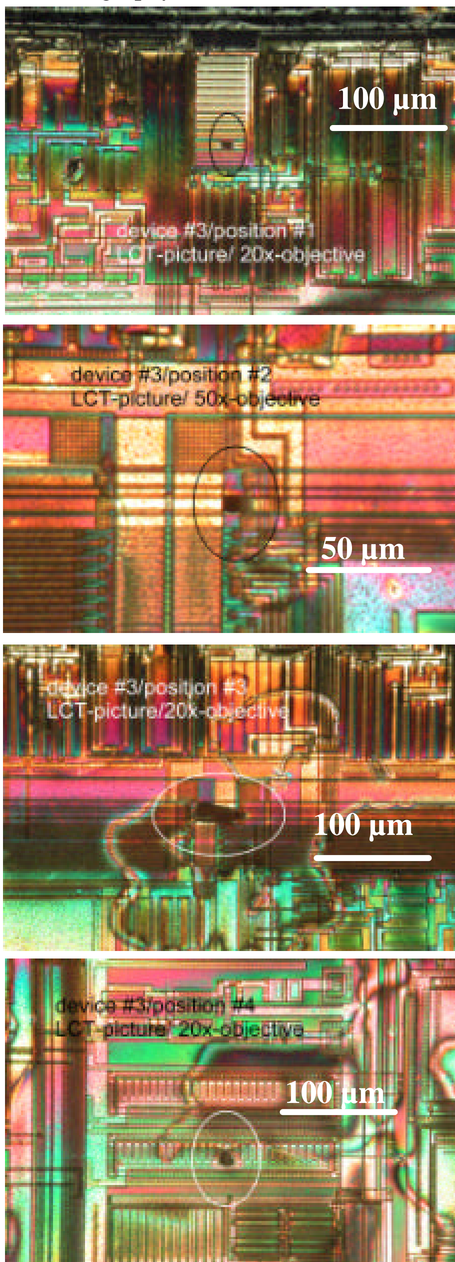

Fig. 8: Liquid crystal images of positions #1... #4 of Fig. 7 in higher magnification

The next comparison is that between IR lock-in thermography and liquid crystal thermography (LCT). Fig. 8 shows LCT images of positions #1, #2 and #3, and #4. In position #5 nothing was observed in LCT. The LCT results generally confirm all IR thermography results, but they also show the limitations of LCT. It is complicated to obtain a homogeneous LC thickness, especially at the die edges there are always some dark positions, which are not wetted. The real spatial resolution of IR thermography is clearly better than that of LCT, though the nominal pixel resolution of LCT is superior. This is due to the non-linear (step-like) contrast behaviour of LCT and to the lateral heat spreading, which disturbs LCT but is suppressed in lock-in thermography. So the IR thermography amplitude images reveal that both in position #3 and #4 there are actually two heat sources, a strong and a weak one. In both cases LCT allowed the detection of either the stronger one, or both merged together, depending on sample temperature.

The final comparison is between IR lock-in thermography and lock-in FMI (fluorescent microthermal imaging). Our experimental lock-in FMI system is not optimized yet to reach highest possible detection sensitivity. Moreover, the applied bias was limited to 10 V here for technical reasons. A problem is also the degradation of the dye limiting the measuring time to about 20 min. Therefore only the heat source in position #4, which was the strongest one, could be investigated by lock-in FMI. Moreover, another device of the same type than that used for the previous investigation was used for this comparison. This device showed the same ESD-induced fault as the previous one, but the primary defect was in a slightly different position. Fig. 9 shows a comparison of the IR lock-in thermography amplitude and its topography image, and the lock-in FMI amplitude image together with its topography image, all measured at Vcc = 10 V. The region imaged in FMI is framed in the IR thermograms. These images are rotated by 180° with respect to Figs. 3, 7, and 8. In this IR amplitude thermogram the brightness scaling was optimized for the dominant defect in position #4, in contrast to the image in Fig. 7. The comparison in Fig. 9 shows that the detection sensitivity of our present experimental lock-in FMI system is still far below that of IR lock-in thermography. However, the spatial resolution of lock-in FMI is clearly superior to that of IR thermography and comparable to that of light emission microscopy. There are some other fault detection techniques like TIVA (Thermal Induced Voltage Alteration) [9] or OBIRCH (Optical Beam Induced Resistance Change) [10], which could not be

compared to lock-in thermography yet, since the authors had no access to these techniques. These techniques rely on changes of the quiescent current on the action of a focused Laser beam. Lock-in thermography could have an advantage to these techniques, since it also allows the detection of weak leakage sites in ICs having a large quiescent current (see Fig. 3).

Conclusions and Outlook

IR lock-in thermography shows a considerably better thermal resolution than previous thermal imaging techniques. This technique has the potential to become a new standard technique for fault localization up to an accuracy of 5 µm. Lock-in thermography may also be used in flip-chip configuration. Other advantages include its ease of operation, since it needs no foreign layer at the surface, no room darkening, the results are straightforward to interpret, and there is no degradation as for FMI.

The comparison between different thermal fault detection techniques has shown that lock-in thermography is able to detect practically all defects, which are visible also in light emission microscopy. We have estimated a detection limit of this thermal technique of below 0.1 mK corresponding to about 3 µW for point heat sources [4] and some 10 µW for slightly extended sources, which is well below the detection limit of liquid crystal thermography. A number of heat sources visible in IR lock-in thermography don't show any light emission, since lock-in thermography detects a different physical mechanism than does LEM. Therefore in some cases, lock-in therography may be more useful, and in other cases LEM may be more useful. Unfortunately, the spatial resolution of IR lock-in thermography is limited to 5 µm because of the IR wavelength of 3 - 5 µm used. Here lock-in FMI may become an interesting alternative in future by detecting local heat sources with sub-micron spatial resolution. The presupposition is, however, that the hitherto unsatisfactory detection sensitivity of lock-in FMI can be considerably improved. Corresponding work is underway.

In future the frequency range of IR lock-in thermography will be extended up to 1 kHz, leading to a further improvement of the effective spatial resolution. Moreover, IR lock-in thermography or lock-in FMI may become integrated into an intelligent IC testing station, which activates and deactivates certain functional groups in the pace of the lock-in correlation. In this way the correct operation of well-defined functional groups in ICs can be tested thermally.

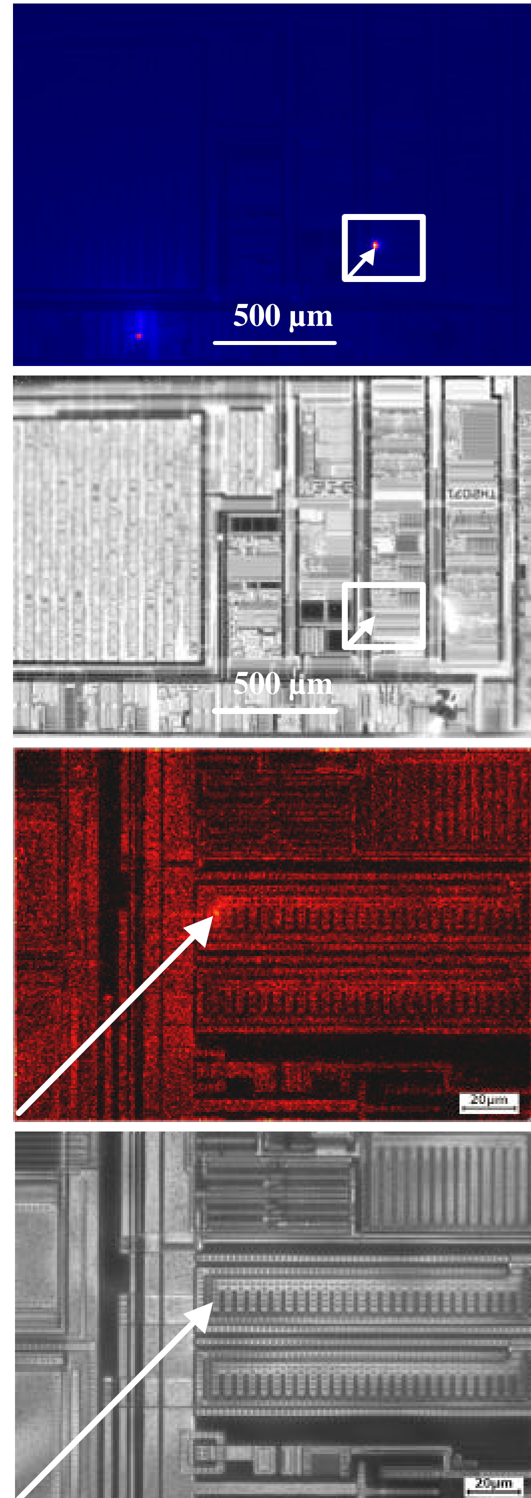

Fig. 9: Lock-in thermography amplitude and topography images (top) and Lock-in FMI amplitude and topography image (bottom) of defect #4 in Fig. 7

Acknowledgements

This work was supported by the BMBF projects No. 0329743B (DIXSI) and KA 0015101AJS0 (FASµm).

References

1. N. Hirayama, K. Nikawa, M. Nakagiri, Proc. ISTFA 1986, pp. 139-144
2. P. Kolodner, J.A. Tyson, Appl. Phys. Lett. **40**, 782 (1982)
3. www.quantumfocus.com
4. O. Breitenstein, M. Langenkamp, F. Altmann, D. Katzer, A. Lindner, H. Eggers, Rev. Sci. Instr. **71**, 4155 (2000)
5. www.thermosensorik.com
6. X.P.V. Maldague: *Theory and Practice of Infrared Technology for Nondestructive Testing*, Wiley (New York) 2001
7. O. Breitenstein, M. Langenkamp, O. Lang, A. Schirrmacher, Solar Energy Materials Solar Cells 65, 55 (2001)
8. www.aim-ir.de
9. www.optomet.com
10. usa.hamamatsu.com